Liu *et al. Energy Mater.* **2025**, *5*, 500068
**DOI:** 10.20517/energymater.2024.235

**Energy Materials**

**Article**

**Open Access**

Check for updates

# Enhanced hydrogen production via coupled methanol oxidation reaction using Pt nanowires as bifunctional electrocatalysts

**Han Liu, Qing-Ling Hong, Yun-Chao Yin*, Feng Shi, Pei Chen, Yu Chen***

Key Laboratory of Macromolecular Science of Shaanxi Province, Shaanxi Key Laboratory for Advanced Energy Devices, Shaanxi Engineering Lab for Advanced Energy Technology, School of Materials Science and Engineering, Shaanxi Normal University, Guodu Street, Chang'an District, Xi'an 710062, China.

***Correspondence to:** Dr. Yun-Chao Yin and Prof. Yu Chen, Key Laboratory of Macromolecular Science of Shaanxi Province, Shaanxi Key Laboratory for Advanced Energy Devices, Shaanxi Engineering Lab for Advanced Energy Technology, School of Materials Science and Engineering, Shaanxi Normal University, Guodu Street, Chang'an District, Xi'an 710062, China. E-mail: yunchaoyin@163.com; ndchenyu@gmail.com

**How to cite this article:** Liu, H.; Hong, Q. L.; Yin, Y. C.; Shi, F.; Chen, P.; Chen, Y. Enhanced hydrogen production via coupled methanol oxidation reaction using Pt nanowires as bifunctional electrocatalysts. *Energy Mater.* **2025**, *5*, 500068. https://dx.doi.org/10.20517/energymater.2024.235

**Received:** 30 Oct 2024 **First Decision:** 28 Nov 2024 **Revised:** 12 Dec 2024 **Accepted:** 19 Dec 2024 **Published:** 7 Mar 2025

**Academic Editor:** Soo Young Kim **Copy Editor:** Ping Zhang **Production Editor:** Ping Zhang

## Abstract

The substitution of oxygen evolution reaction with a thermodynamically favorable small molecule oxidation reaction offers a compelling pathway toward efficient and energy-conserving production of clean hydrogen fuel. Here, we report the rational design and synthesis of ultra-long Pt nanowires (NWs) featuring specific crystal facets, which act as bifunctional electrocatalysts for both the hydrogen evolution reaction (HER) and methanol oxidation reaction (MOR) under alkaline electrolyte. Pt NWs exhibited remarkable performance, requiring only 0.61 V to obtain 10 mA $cm^{-2}$ when coupling HER with MOR, substantially lower than the 1.76 V demanded for traditional water splitting. The excellent HER and MOR performance could be primarily attributed to the unique one-dimensional structural characteristics, distinctive crystal facets, and increased specific surface area of the Pt NWs. This research underscores the significance of developing bifunctional electrocatalysts, thereby contributing to the ongoing efforts to advance efficient and energy-conserving hydrogen production.

**Keywords:** Pt nanowires, bifunctional electrocatalyst, hydrogen evolution reaction, methanol oxidation reaction

## INTRODUCTION

Hydrogen ($H_2$) is often celebrated as one of the leading candidates for future energy systems, primarily because of its impressive energy density and minimal environmental impact[1-3]. However, conventional hydrogen production via steam reforming operates under high-temperature and high-pressure conditions, inevitably generating carbon monoxide (CO) impurities[4]. These impurities can quickly degrade catalytic performance by causing poisoning and rapid deactivation. Alternatively, hydrogen production through electrocatalytic water splitting is seen as a cleaner, more efficient, and sustainable method compared to traditional steam reforming techniques[5-9]. While the promise of large-scale hydrogen production through electrochemical water splitting is evident, several significant challenges remain[10-13]. A primary concern is the substantial energy costs associated with electrical consumption. Moreover, the oxygen evolution reaction (OER) and hydrogen evolution reaction (HER) are intricately linked, potentially leading to the dangerous formation of explosive $O_2/H_2$ mixtures caused by gas crossover. Furthermore, the presence of oxygen poses a threat of generating reactive oxygen species, which can adversely affect membrane integrity and compromise system longevity.

Addressing these limitations through the integration of small-molecule electrolytes in the anode compartment provides a compelling alternative[14-17]. When juxtaposed with conventional electrocatalytic water splitting, the process of hydrogen generation through small-molecule oxidation systems boasts three primary benefits: (i) a notable increase in overall energy conversion efficiency, which translates to low energy expense; (ii) the enhanced safety due to the elimination of $O_2$ contamination, thereby reducing the risk of explosive mixtures; and (iii) the removal of membranes since $O_2$ production at the anode is circumvented[18,19]. This strategy not only significantly lowers operational costs but also mitigates stability issues linked to the finite lifespan of membranes[20,21]. The methanol oxidation-assisted hydrogen evolution process, which replaces the OER with methanol oxidation reaction (MOR), has garnered considerable attention as a promising strategy for producing hydrogen efficiently. Remarkably, the theoretical voltage required for this process is merely 0.016 V[22]. Furthermore, when factoring in the production costs of methanol, this method offers the potential for nearly a 50% reduction in energy usage[23-26]. Thus, there is an increasing focus on MOR-assisted water splitting, driving the ongoing advancement of essential catalytic materials[27]. In light of these developments, there is a pressing need for a high-performance bifunctional electrocatalyst that can effectively accelerate MOR and HER kinetics.

Pt-based materials represent the most promising candidates for MOR-assisted electrocatalytic water splitting due to their superior activity and stability for both HER and MOR[28]. However, the electrocatalytic performance of commercial Pt electrocatalysts is primarily limited by the small number of active sites and a propensity for aggregation[29]. Furthermore, the scarcity and high cost of Pt remain critical challenges to its widespread practical application[30]. A promising solution lies in the design of Pt nanowires (NWs) with a one-dimensional (1D) nanostructure[31-36]. These 1D Pt NWs offer a high specific surface area, which not only enhances electrocatalytic activity but also improves Pt utilization, thereby reducing the overall cost in practical applications.

Here, we successfully synthesized ultrafine Pt NWs with a diameter of 2.39 nm using an iodide-assisted one-pot method. The roles of iodide ions, polyvinylpyrrolidone (PVP), and CO in directing the formation of Pt NWs were systematically investigated. The resulting Pt NWs exhibit outstanding bifunctional catalytic performance for MOR and HER. The significant enhancement in performance is primarily attributed to the favorable 1D morphology, unique crystal facets, and large specific surface area of the NWs. Furthermore, we design and construct a two-electrode cell to evaluate the process of methanol oxidation-assisted hydrogen production. The results demonstrate that the energy input required for the MOR-assisted water-splitting

system is substantially lower than that of conventional water-splitting systems. Additionally, compared to Pt black as a bifunctional catalyst, Pt NWs significantly reduce the voltage required for methanol oxidation-assisted hydrogen production. These findings underscore the ability of the 1D NW structure to optimize reaction sites, thereby enhancing catalytic activity.

## EXPERIMENTAL

### Chemical

Platinum acetylacetonate ($Pt(acac)_2$, ≥ 0.98), potassium hydroxide (KOH, ≥ 0.85), N,N-dimethylformamide (DMF, ≥ 0.99), potassium iodide (KI, ≥ 99.0%), PVP (K30), and Nafion (5.0 wt%) were procured from Sinopharm. Pt black electrocatalyst was sourced from Johnson Matthey.

### Synthesis of Pt NWs

To the reaction vessel, 0.15 mmol of $Pt(acac)_2$, 300 mg of PVP, 0.75 mmol of KI, and 30 mL of DMF were added. CO was introduced until saturation, and the mixture was then reacted at 130 °C for 6 h. Subsequently, the product was immersed in KOH for 12 h to facilitate thorough rinsing and purification. The influence of reaction time, iodide ions, PVP, and CO on the morphology of the reaction products was systematically investigated through a series of experiments.

### Electrochemical measurements

The HER and MOR activity of the electrocatalysts were initially evaluated using a three-electrode configuration. The procedure employs carbon rods, Hg/HgO electrodes, and working electrodes modified with Pt NWs. First, 2 mg of Pt NWs were mixed with 1 mL of water and isopropanol in a 4:1 volume ratio and sonicated for 30 min to obtain a uniform material ink. Subsequently, 4 μL of the ink was meticulously deposited onto the working electrode, followed by the addition of 4 μL of Nafion (0.05 wt%). All potentials were converted to the reversible hydrogen electrode (RHE): $E_{RHE} = E_{Hg/HgO} + 0.095 + 0.059 \times pH$.

The electrochemical surface area (ECSA) of Pt NWs was determined using the hydrogen adsorption/desorption charge current as a reference, as given in:

$$\mathrm{ECSA} = \frac{Q_{Pt}}{Q_{ref} \times m_{Pt}}$$

Where $Q_{Pt}$ denotes the average charge of the hydrogen adsorption/desorption region, $Q_{ref}$ = 210 μC·cm$^{-2}$ and $m_{Pt}$ represents the Pt loading mass. CO stripping voltammetry was conducted in a 1 mol·L$^{-1}$ KOH solution. Initially, CO was introduced into the solution and held at -1 V to ensure complete adsorption on the crystal surface. Excess CO in the electrolyte was then removed by purging with nitrogen gas. The CO stripping experiment was subsequently performed within the potential range of 0 V to 1.2 V.

### Characterizations

Structural characterization was conducted using X-ray diffraction (XRD). Surface properties of the materials were assessed using X-ray photoelectron spectroscopy (XPS) with a PHI 5000 VersaProbe III. For transmission electron microscopy (TEM), assessments were conducted using TECNAI G2 F20 and HT7800.

## RESULTS AND DISCUSSION

### Synthesis and characterization of Pt NWs

To synthesize the materials, a solution comprising Pt precursor, KI, and PVP was prepared in DMF. Subsequently, saturated CO was introduced, and the reaction was conducted at 130 °C for a specified duration to yield Pt NWs [Figure 1]. The morphology of Pt NWs was thoroughly examined through TEM.

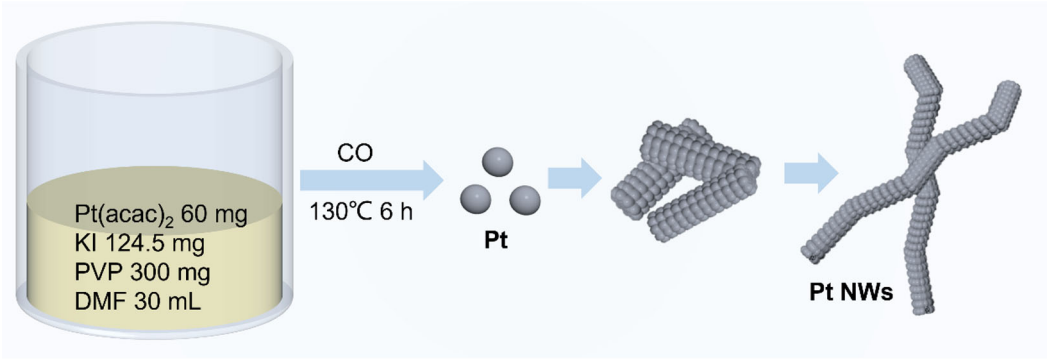


**Figure 1.** Schematic representation of the synthesis of Pt NWs. NWs: Nanowires.

As illustrated in Figure 2A, these NWs display a uniform diameter of 2.39 nm [Supplementary Figure 1]. Moreover, the surface of Pt NWs is predominantly characterized by the Pt (200) and Pt (111) crystal planes [Figure 2B-E][37]. Additionally, the Pt NWs exhibit a polycrystalline architecture, with the corresponding diffraction rings clearly observable [Figure 2F]. To assess the uniformity of the synthesized material, we characterized the microscopic morphology of both individual NWs at various locations and NWs. As depicted in Supplementary Figure 2, the diameter of the same NW remains consistent across multiple locations, approximately 2.39 nm, with its surface predominantly exposing the Pt (200) and Pt (111) planes. Similarly, the diameters of different NWs are also approximately 2.39 nm, and the exposed crystal planes are uniformly aligned. These observations underscore the remarkable uniformity of the synthesized NWs. Concurrently, Pt NWs display distinct XRD peaks at 39.7°, 46.2°, 67.5°, and 81.3° (Pt#04-0802) [Figure 2G]. Simultaneously, the oxidation states of the surface elements in the Pt NWs were examined using XPS. The Pt 4f spectrum reveals peaks attributable to metallic Pt and $Pt^{2+}$ [Figure 2H][38]. As a comparison, the morphology of commercial Pt black is characterized by typical nanoparticles, with the surface primarily composed of Pt (111) and Pt (200) crystal planes [Supplementary Figure 3].

To elucidate the formation process of Pt NWs, a series of comparative experiments was conducted. The role of iodide ions in the reaction was first investigated by analyzing the morphology of reaction products under varying iodide ion concentrations, while maintaining constant reaction time and temperature. As illustrated in Figure 3A, in the absence of iodide ions, the products predominantly comprised nanoparticles alongside a minor fraction of nanorods. Upon the addition of iodide ions (I:Pt = 1.25), the rod-like morphology began to prevail [Figure 3B]. Further increases in iodide ion concentration facilitated the gradual formation of NWs, achieving an ideal NW structure at I:Pt = 5 [Figure 3C and D]. These phenomena indicate the critical role of iodide ions in driving NW formation. Studies reveal that the roles of iodide ions can be categorized into two main aspects: first, they form Pt-I compounds with the Pt precursor, and their reduction kinetics differ from those of the Pt precursor, which induces the oriented growth of Pt materials; second, iodide ions act as capping agents, strongly adsorbing onto the Pt surface, thereby further promoting the directional growth of Pt. Meanwhile, the roles of CO and PVP in the synthesis of Pt NWs are systematically investigated. Under the optimized conditions for Pt NW synthesis, the absence of CO predominantly yields nanoparticles rather than NWs, underscoring the critical role of CO in guiding the formation of the desired NW morphology [Supplementary Figure 4A]. Similarly, the impact of PVP was examined. As shown in Supplementary Figure 4B, the absence of PVP also results in the formation of nanoparticles instead of NWs, highlighting the indispensable role of PVP in facilitating the synthesis of Pt NWs. The growth dynamics of Pt NWs are further explored under optimized conditions. After one hour of reaction, uniform Pt nanoparticles are predominant [Figure 3E]. As the reaction time extended, shorter NW structures emerged [Figure 3F and G], and after six hours, the products exhibited uniformly elongated NWs [Figure 3H].

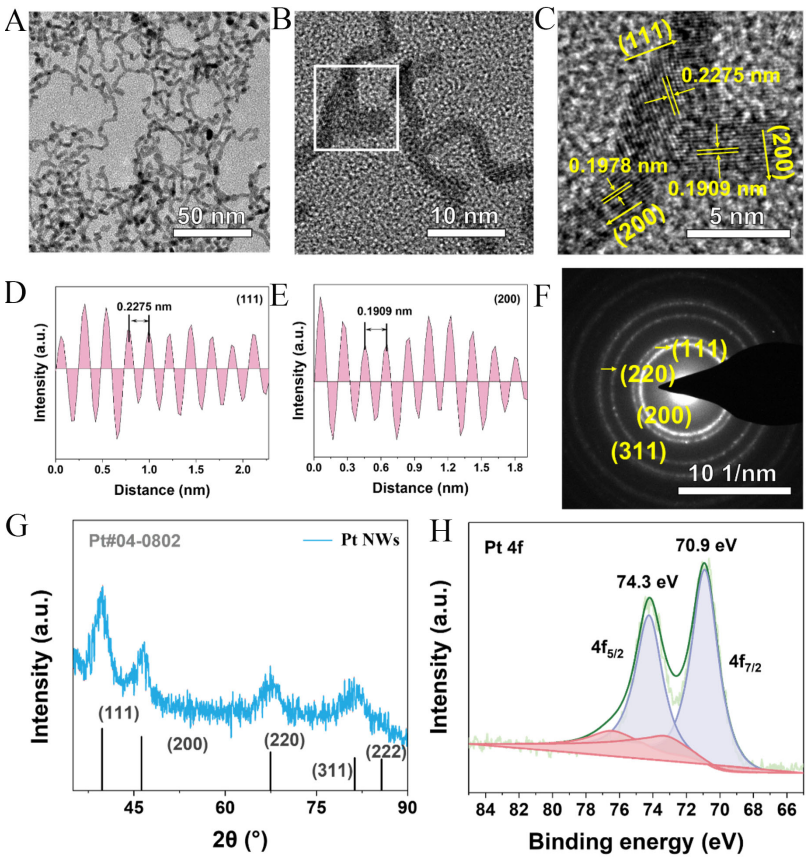


**Figure 2.** (A) TEM image of Pt NWs; (B and C) A HRTEM image of Pt NWs; (D and E) Distribution of crystal plane spacing; (F) SAED data of Pt NWs; (G) XRD of Pt NWs; (H) XPS Pt 4f spectrum of Pt NWs. TEM: Transmission electron microscopy; NWs: nanowires; XRD: X-ray diffraction; XPS: X-ray photoelectron spectroscopy; HRTEM: high-resolution transmission electronmicroscopy; SAED: selected area electron diffraction.

Additionally, to assess the impact of extended reaction times on the morphology, the reaction time was increased to 24 h [Supplementary Figure 5]. The results showed that the morphology remained largely consistent with that observed at six hours. Therefore, to optimize the efficiency of Pt NW synthesis, six hours was selected as the optimal reaction time.

### HER activity of Pt NWs

The electrocatalytic activity of Pt NWs for HER was first evaluated in a three-electrode configuration. This assessment was conducted in $N_2$-saturated 1 M KOH solution [Figure 4A]. Cyclic voltammetry (CV) measurements for Pt NWs, commercial Pt black and Pt/C reveal comparable electrochemical behavior [Figure 4B and Supplementary Figure 6A]. Notably, Pt NWs exhibit more pronounced electrochemical reduction peaks than Pt black within 0-0.5 V, indicating a higher active surface area for the former. Moreover, Pt NWs exhibit superior electrocatalytic performance compared to Pt black and Pt/C at equivalent current densities [Figure 4C and D, Supplementary Figure 6B]. The Tafel plots for the samples were derived by fitting the Linear Sweep Voltammetry (LSV) curves associated with their HER performance. The Tafel slope for Pt NWs was determined to be 48.8 mV·dec$^{-1}$, in contrast to 52.1 mV·dec$^{-1}$ for Pt black, underscoring the enhanced electrocatalytic activity of Pt NWs for HER [Figure 4E]. Furthermore, the stability of Pt NWs in alkaline electrolytes was assessed via chronoamperometry (CA). As depicted in Figure 4F, the current density for Pt NWs exhibits minimal degradation over time, outperforming commercial Pt black in maintaining HER activity. This observation underscores the superior

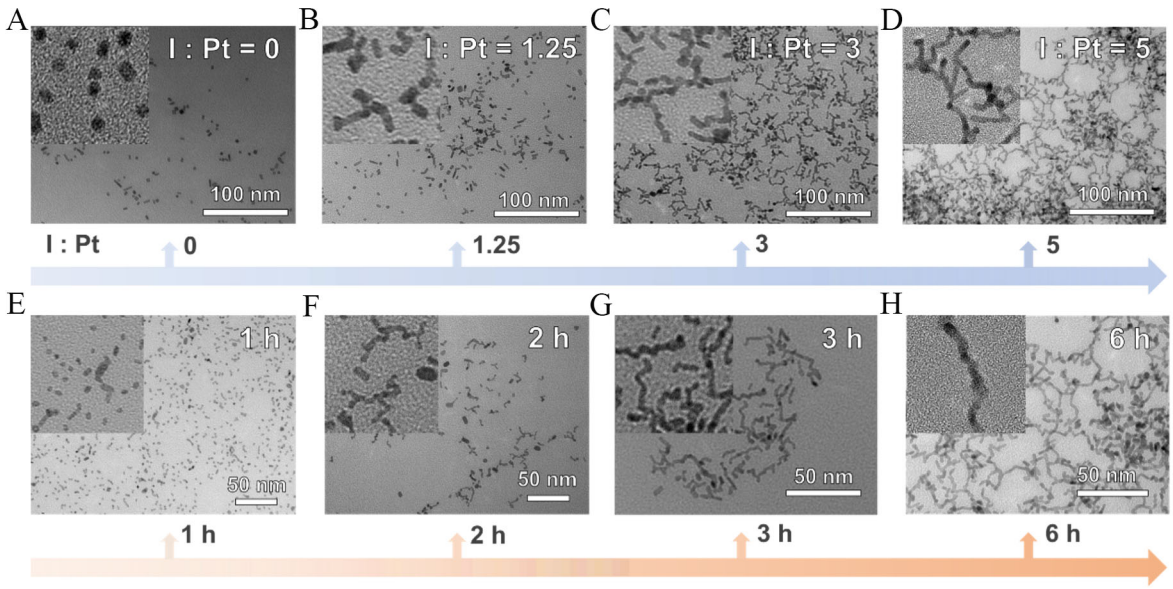


**Figure 3.** (A-D) TEM images of Pt nanostructures synthesized using 300 mg of PVP and saturated CO under varying iodide ion concentrations; (E-H) TEM images of reaction products obtained at different time intervals from the reaction between 300 mg of PVP, saturated CO and 124.5 mg of KI. TEM: Transmission electron microscopy; PVP: polyvinylpyrrolidone.

stability of Pt NWs in facilitating the HER under alkaline conditions. The hydrogen production of Pt NWs at various voltages was quantitatively analyzed using chromatography. In nitrogen-saturated alkaline electrolytes, the hydrogen yield increases with decreasing applied voltages [Supplementary Figure 7].

### MOR activity of Pt NWs

The electrocatalytic performance of the catalysts toward MOR was systematically assessed by CV. Pt NWs exhibit an onset potential ($E_{onset}$) of 0.41 V, markedly lower than that of Pt black (0.48 V) and Pt/C (0.42 V), highlighting a more favorable MOR kinetics for Pt NWs [Figure 5A and Supplementary Figure 8]. The ECSA for each electrocatalyst was determined through the underpotential deposition of $H^+$ on Pt surfaces [Supplementary Figure 9]. Pt NWs demonstrate an ECSA of 39.01 $m^2 g^{-1}$, substantially exceeding that of commercial Pt black (20.98 $m^2 g^{-1}$), which is attributed to the enhanced atomic exposure afforded by the 1D morphology of Pt NWs. As shown in Figure 5B, Pt NWs achieve a mass activity of 1.55 A $mg^{-1}$, approximately 2.6-fold greater than Pt black (0.59 A $mg^{-1}$), with a specific activity of 4.07 mA $cm^{-2}$, surpassing that of Pt black (2.61 mA $cm^{-2}$, Supplementary Figure 10). These findings underscore the capacity of the 1D architecture to elevate the catalytic efficacy of Pt-based materials. A comparative summary of MOR activity for various electrocatalysts from recent studies is presented in Table 1, clearly highlighting the superior performance of our 1D Pt NWs. Collectively, these results demonstrate the potential of 1D structuring to significantly enhance electrocatalytic activity. The stability of the electrocatalysts was evaluated using CA at 0.77 V. Both Pt NWs and Pt black exhibit an initial rapid decrease in current, a behavior attributed to the diffusion-controlled characteristics of the CA, in which current scales directly with reactant concentration[51]. As the reaction progresses, methanol molecules on the electrode surface are consumed, resulting in a decrease in current. However, this drop is also influenced by the adsorption of CO* on the Pt surface, which can decelerate the rate of current density reduction. The current density decay for Pt NWs is significantly less pronounced than that for Pt black, indicating superior catalytic performance of Pt NWs in the methanol oxidation process compared to commercial Pt black [Figure 5C]. The crystalline phase and microstructural morphology of the samples were examined after stability testing. The results reveal that the crystalline phase retains the characteristic face-centered cubic

**Table 1. A summary of the performance of Pt-based electrocatalysts for the MOR**

| Catalysts | Electrolyte | Mass activity (A $mg^{-1}$) | Specific activity (mA $cm^{-2}$) | Ref. |
|---|---|---|---|---|
| Pt NWs | 1 M KOH + 0.5 M $CH_3OH$ | 1.55 | 4.07 | This work |
| Pt black | 1 M KOH + 0.5 M $CH_3OH$ | 0.59 | 2.61 | This work |
| $Pt/Ni(OH)_2$/rGO-4 | 1 M KOH + 1 M $CH_3OH$ | 1.24 | 1.94 | [39] |
| PtZn/MWNT | 0.1 M KOH + 0.5 M $CH_3OH$ | 0.54 | 1.14 | [40] |
| PtAuRu/RGO | 1 M KOH + 1 M $CH_3OH$ | 1.6 | - | [41] |
| PtPdRhAg nanoframes | 0.5 M KOH + 2 M $CH_3OH$ | 1.2 | - | [42] |
| AgAu@Pt nanoframes | 0.2 M KOH + 1 M $CH_3OH$ | 0.48 | 1.96 | [43] |
| Pd@Pt/rGO | 0.5 M KOH + 0.5 M $CH_3OH$ | 1.2 | - | [44] |
| Pd@PtNi nanostructures | 1 M KOH + 1 M $CH_3OH$ | 1.6 | 2.68 | [45] |
| Porous Pt nanotubes | 1 M KOH + 1 M $CH_3OH$ | 2.3 | 4.9 | [46] |
| $CeO_2$/PtBi nanoparticles | 1 M KOH + 1 M $CH_3OH$ | 6.83 | 29.42 | [47] |
| PtNi/NbN-C | 1 M KOH + 1 M $CH_3OH$ | 6.03 | 105.3 | [48] |
| PtCu nanoframes | 0.5 M KOH, 1 M $CH_3OH$ | 2.26 | 18.2 | [49] |
| Pt nanowires | 1 M KOH + 1 M $CH_3OH$ | 4.5 | 10.9 | [50] |

MOR: Methanol oxidation reaction.

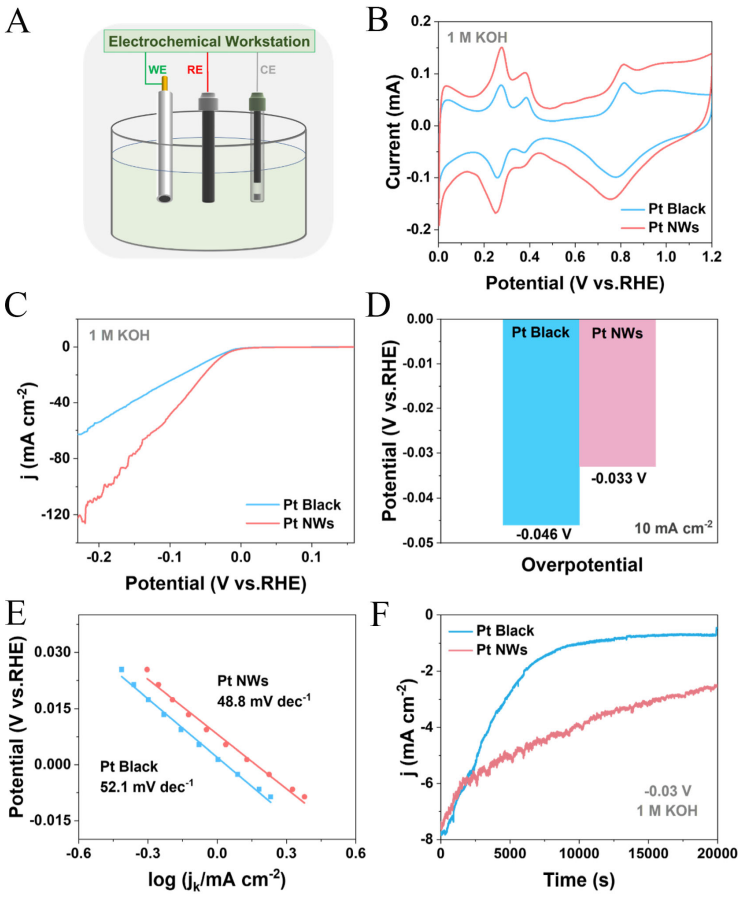


**Figure 4.** (A) A schematic representation of the three-electrode electrochemical testing configuration; (B) CV profile of the catalysts; (C) LSV curves of Pt NWs and Pt black; (D) Comparison of overpotentials across various materials; (E) Corresponding Tafel plots of Pt NWs and Pt black; (F) i-t curves for the electrocatalysts in HER. CV: Cyclic voltammetry; LSV: linear sweep voltammetry; NWs: nanowires; HER: hydrogen evolution reaction.

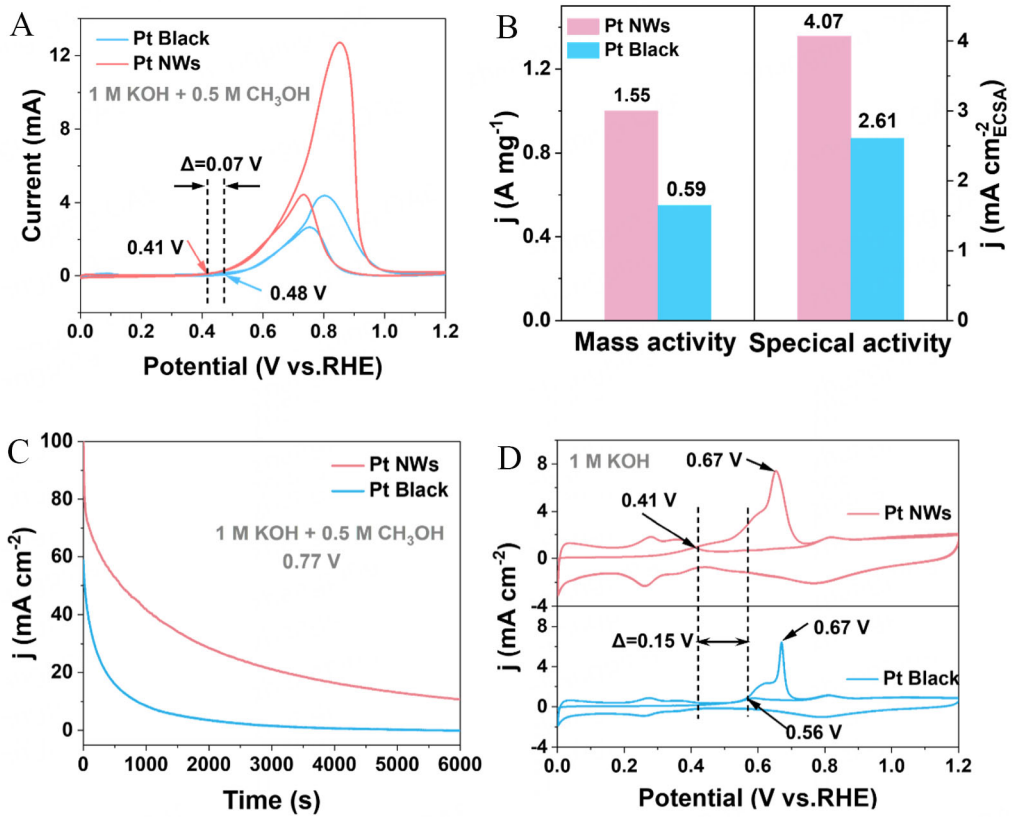


**Figure 5.** (A) CV profiles of Pt NWs and Pt black in 1 M KOH containing 0.5 M $CH_3OH$; (B) Comparison of the catalytic activities of Pt NWs and Pt black; (C) CA stability curves of the catalysts; (D) CO stripping voltammetry profiles. CV: Cyclic voltammetry; NWs: nanowires.

(fcc) structure of Pt without any detectable alterations, and the NW morphology is fully preserved [Supplementary Figure 11].

CO stripping experiments were performed to elucidate the resistance of electrocatalysts to poisoning, a critical factor for MOR performance. CO, as an intermediate in the methanol oxidation process, readily adsorbs onto active sites during the reaction, resulting in catalytic activity attenuation. The $E_{onset}$ for CO oxidation on Pt NWs is measured at 0.41 V, notably lower than the 0.56 V observed for commercial Pt black [Figure 5D]. These results further validate the improved anti-poisoning characteristics and overall catalytic efficiency of Pt NWs for MOR.

### MOR-assisted water splitting

Building on the high activity of Pt NWs for both HER and MOR, we utilized Pt NWs as the anode and cathode to investigate methanol-assisted HER [Figure 6A]. LSV polarization curves were recorded for hydrogen production under various anode-cathode configurations and electrolyte conditions [Figure 6B]. In the absence of methanol, the Pt NW sample obtained 10 mA $cm^{-2}$ at 1.76 V; conversely, in the methanol-containing system, this current density was realized at a significantly lower voltage of 0.61 V. This finding demonstrates that integrating the methanol oxidation process can effectively reduce the total energy input necessary for water electrolysis. Moreover, when compared to the Pt black system, it was observed that Pt NWs require a lower voltage to achieve the targeted current density. This enhancement is primarily attributed to the 1D structural characteristics of Pt NWs, which optimizes the exposure of active sites and

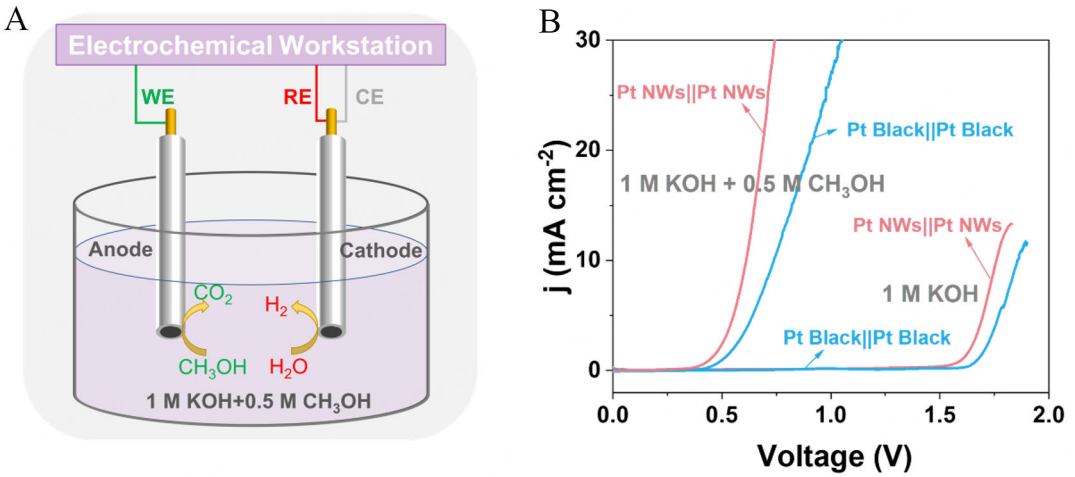


**Figure 6.** (A) A schematic representation of the two-electrode electrochemical testing configuration; (B) LSV curves for Pt NWs and Pt black. LSV: Linear sweep voltammetry; NWs: nanowires.

boosts the catalytic efficiency of Pt for both HER and MOR.

## CONCLUSIONS

We synthesized ultra-long Pt NWs as bifunctional electrocatalysts for HER and MOR in alkaline environments. These NWs demonstrated remarkable bifunctional properties for both MOR and HER, demonstrating significantly enhanced performance. This enhancement can be primarily attributed to their advantageous 1D morphology, unique crystal facets, and extensive surface area. To exploit their capabilities, we employed Pt NWs as the cathode for HER and the anode for MOR within a two-electrode configuration, facilitating the production of high-value hydrogen at room temperature with minimal energy input. Under methanol-assisted conditions, the system achieved 10 $mAcm^{-2}$ with an overpotential of only 0.61 V, significantly lower than that required in systems devoid of methanol assistance. These findings represent a significant advancement in industrial strategies for the energy-efficient and sustainable production of clean hydrogen.

## DECLARATIONS

### Authors' contributions

Made substantial contributions to the conception and design of the study and performed data analysis and interpretation: Liu, H.

Made substantial contributions to the conception and design of the study: Hong, Q. L.

Contributed to research concept generation, research funding acquisition, resource collection, experimental design and verification, research topic supervision and guidance, and paper review and revision: Yin, Y..C.; Chen, Y.; Shi, F.; Chen, P.

### Availability of data and materials

The raw data supporting the findings of this study are available in this article and its Supplementary Materials. Additional data can be obtained from the corresponding authors upon request. Detailed materials and methods are provided in the Supplementary Materials. All datasets generated for this study are included in the article and Supplementary Materials.

**Financial support and sponsorship**

This research was sponsored by the National Natural Science Foundation of China (22272103), Science and Technology Innovation Team of Shaanxi Province (2023-CX-TD-27), and Sanqin Scholar Innovation Teams in Shaanxi Province, China.

**Conflicts of interest**

All authors declared that there are no conflicts of interest.

**Ethical approval and consent to participate**

Not applicable.

**Consent for publication**

Not applicable.



## REFERENCES

1. Tian, X.; Zhao, X.; Su, Y. Q.; et al. Engineering bunched Pt-Ni alloy nanocages for efficient oxygen reduction in practical fuel cells. *Science* **2019**, *366*, 850-6. DOI
2. Lin, L.; Zhou, W.; Gao, R.; et al. Low-temperature hydrogen production from water and methanol using Pt/α-MoC catalysts. *Nature* **2017**, *544*, 80-3. DOI
3. Zhang, X.; Luo, Z.; Yu, P.; et al. Lithiation-induced amorphization of $Pd_3P_2S_8$ for highly efficient hydrogen evolution. *Nat. Catal.* **2018**, *1*, 460-8. DOI
4. Yukesh, K. R.; Kavitha, S.; Preethi; et al. Techno-economic assessment of various hydrogen production methods - a review. *Bioresour. Technol.* **2021**, *319*, 124175. DOI
5. Mahmood, J.; Li, F.; Jung, S. M.; et al. An efficient and pH-universal ruthenium-based catalyst for the hydrogen evolution reaction. *Nat. Nanotechnol.* **2017**, *12*, 441-6. DOI
6. Staffell, I.; Scamman, D.; Velazquez, A. A.; et al. The role of hydrogen and fuel cells in the global energy system. *Energy. Environ. Sci.* **2019**, *12*, 463-91. DOI
7. Morales-Guio, C. G.; Stern, L. A.; Hu, X. Nanostructured hydrotreating catalysts for electrochemical hydrogen evolution. *Chem. Soc. Rev.* **2014**, *43*, 6555-69. DOI PubMed
8. Amano, F.; Tsushiro, K. Proton exchange membrane photoelectrochemical cell for water splitting under vapor feeding. *Energy. Mater.* **2024**, *4*, 400006. DOI
9. Ma, Y.; Wang, L.; Zhao, W.; et al. Reactant enrichment in hollow void of Pt NPs@MnOx nanoreactors for boosting hydrogenation performance. *Natl. Sci. Rev.* **2023**, *10*, nwad201. DOI PubMed PMC
10. Xiao, X.; Yang, L.; Sun, W.; et al. Electrocatalytic water splitting: from harsh and mild conditions to natural seawater. *Small* **2022**, *18*, e2105830. DOI
11. Zhang, X.; Guo, Y.; Wang, C. Multi-interface engineering of nickel-based electrocatalysts for alkaline hydrogen evolution reaction. *Energy. Mater.* **2024**,. DOI
12. Rausch, B.; Symes, M. D.; Chisholm, G.; Cronin, L. Decoupled catalytic hydrogen evolution from a molecular metal oxide redox mediator in water splitting. *Science* **2014**, *345*, 1326-30. DOI PubMed
13. Nikolaidis, P.; Poullikkas, A. A comparative overview of hydrogen production processes. *Renew. Sustain. Energy. Rev.* **2017**, *67*, 597-611. DOI
14. Oh, Y.; Theerthagiri, J.; Aruna, K. M.; Min, A.; Moon, C. J.; Choi, M. Y. Electrokinetic-mechanism of water and furfural oxidation on pulsed laser-interlaced $Cu_2O$ and CoO on nickel foam. *J. Energy. Chem.* **2024**, *91*, 145-54. DOI
15. Wang, T.; Tao, L.; Zhu, X.; et al. Combined anodic and cathodic hydrogen production from aldehyde oxidation and hydrogen evolution reaction. *Nat. Catal.* **2022**, *5*, 66-73. DOI
16. Liu, X.; Jiang, Y.; Huang, J.; et al. Bifunctional PdPt bimetallenes for formate oxidation-boosted water electrolysis. *Carbon. Energy.* **2023**, *5*, e367. DOI
17. Ge, Z.; Ding, Y.; Wang, T.; et al. Interfacial engineering of holey platinum nanotubes for formic acid electrooxidation boosted water splitting. *J. Energy. Chem.* **2023**, *77*, 209-16. DOI
18. Li, Y.; Wei, X.; Chen, L.; Shi, J. Electrocatalytic hydrogen production trilogy. *Angew. Chem. Int. Ed.* **2021**, *60*, 19550-71. DOI
19. Song, Y.; Ji, K.; Duan, H.; Shao, M. Hydrogen production coupled with water and organic oxidation based on layered double hydroxides. *Exploration* **2021**, *1*, 20210050. DOI PubMed PMC

20. Lee, H.; Theerthagiri, J.; Aruna, K. M.; et al. Leveraging phosphate group in Pd/PdO decorated nickel phosphate microflowers via pulsed laser for robust hydrogen production in hydrazine-assisted electrolyzer. *Int. J. Hydrogen. Energy.* **2024**, *57*, 176-86. DOI
21. Jeong, Y.; Naik, S. S.; Theerthagiri, J.; et al. Manifolding surface sites of compositional CoPd alloys via pulsed laser for hydrazine oxidation-assisted energy-saving electrolyzer: activity origin and mechanism discovery. *Chem. Eng. J.* **2023**, *470*, 144034. DOI
22. Sun, H.; Kim, H.; Song, S.; Jung, W. Copper foam-derived electrodes as efficient electrocatalysts for conventional and hybrid water electrolysis. *Mater. Rep. Energy.* **2022**, *2*, 100092. DOI
23. Yang, F.; Qiao, W.; Yu, L.; Wang, S.; Feng, L. Support engineering modulated Pt/hierarchical $MoSe_2$@mesoporous hollow carbon spheres for efficient methanol-assisted water splitting. *Chem. Eng. J.* **2024**, *483*, 149055. DOI
24. Ding, M.; Chen, Z.; Liu, C.; et al. Electrochemical $CO_2$ reduction: progress and opportunity with alloying copper. *Mater. Rep. Energy.* **2023**, *3*, 100175. DOI
25. Qiao, W.; Yu, L.; Chang, J.; Yang, F.; Feng, L. Efficient bi-functional catalysis of coupled $MoSe_2$ nanosheet/Pt nanoparticles for methanol-assisted water splitting. *Chin. J. Catal.* **2023**, *51*, 113-23. DOI
26. Muthumeenal, A.; Pethaiah, S. S.; Nagendran, A. Investigation of SPES as PEM for hydrogen production through electrochemical reforming of aqueous methanol. *Renew. Energy.* **2016**, *91*, 75-82. DOI
27. Liu, C.; Feng, L. Advances in anode catalysts of methanol-assisted water-splitting reactions for hydrogen generation. *Chin. J. Struct. Chem.* **2023**, *42*, 100136. DOI
28. Qiao, W.; Huang, X.; Feng, L. Advances of PtRu-based electrocatalysts for methanol oxidation. *Chin. J. Struct. Chem.* **2022**, *41*, 2207016-34. DOI
29. Cui, C.; Gan, L.; Heggen, M.; Rudi, S.; Strasser, P. Compositional segregation in shaped Pt alloy nanoparticles and their structural behaviour during electrocatalysis. *Nat. Mater.* **2013**, *12*, 765-71. DOI PubMed
30. Zheng, Y.; Jiao, Y.; Vasileff, A.; Qiao, S. Z. The hydrogen evolution reaction in alkaline solution: from theory, single crystal models, to practical electrocatalysts. *Angew. Chem. Int. Ed.* **2018**, *57*, 7568-79. DOI PubMed
31. Xie, Y.; Cai, J.; Wu, Y.; et al. Boosting water dissociation kinetics on Pt-Ni nanowires by N-induced orbital tuning. *Adv. Mater.* **2019**, *31*, e1807780. DOI
32. Li, H. H.; Zhao, S.; Gong, M.; et al. Ultrathin PtPdTe nanowires as superior catalysts for methanol electrooxidation. *Angew. Chem. Int. Ed.* **2013**, *52*, 7472-6. DOI
33. Kariuki, N. N.; Khudhayer, W. J.; Karabacak, T.; Myers, D. J. Glad Pt-Ni alloy nanorods for oxygen reduction reaction. *ACS. Catal.* **2013**, *3*, 3123-32. DOI
34. Yang, F.; Ren, R.; Zhang, X.; et al. Tailoring the electronic structure of PdAg*x* alloy nanowires for high oxygen reduction reaction. *Chin. J. Struct. Chem.* **2023**, *42*, 100068. DOI
35. Sun, B.; Jiang, Y.; Hong, Q.; et al. Pt-Te alloy nanowires towards formic acid electrooxidation reaction. *J. Energy. Chem.* **2023**, *85*, 481-9. DOI
36. Theerthagiri, J.; Karuppasamy, K.; Lee, S. J.; et al. Fundamentals and comprehensive insights on pulsed laser synthesis of advanced materials for diverse photo- and electrocatalytic applications. *Light. Sci. Appl.* **2022**, *11*, 250. DOI PubMed PMC
37. Huang, Z.; Cheng, T.; Shah, A. H.; et al. Edge sites dominate the hydrogen evolution reaction on platinum nanocatalysts. *Nat. Catal.* **2024**, *7*, 678-88. DOI
38. Zhu, Y.; Zhu, X.; Bu, L.; et al. Single-atom in-doped subnanometer Pt nanowires for simultaneous hydrogen generation and biomass upgrading. *Adv. Funct. Mater.* **2020**, *30*, 2004310. DOI
39. Huang, W.; Wang, H.; Zhou, J.; et al. Highly active and durable methanol oxidation electrocatalyst based on the synergy of platinum-nickel hydroxide-graphene. *Nat. Commun.* **2015**, *6*, 10035. DOI
40. Qi, Z.; Xiao, C.; Liu, C.; et al. Sub-4 nm PtZn Intermetallic nanoparticles for enhanced mass and specific activities in catalytic electrooxidation reaction. *J. Am. Chem. Soc.* **2017**, *139*, 4762-8. DOI
41. Ren, F.; Wang, C.; Zhai, C.; et al. One-pot synthesis of a RGO-supported ultrafine ternary PtAuRu catalyst with high electrocatalytic activity towards methanol oxidation in alkaline medium. *J. Mater. Chem. A.* **2013**, *1*, 7255. DOI
42. Saleem, F.; Ni, B.; Yong, Y.; Gu, L.; Wang, X. Ultra-small tetrametallic Pt-Pd-Rh-Ag nanoframes with tunable behavior for direct formic acid/methanol oxidation. *Small* **2016**, *12*, 5261-8. DOI
43. Yan, X.; Yu, S.; Tang, Y.; Sun, D.; Xu, L.; Xue, C. Triangular AgAu@Pt core-shell nanoframes with a dendritic Pt shell and enhanced electrocatalytic performance toward the methanol oxidation reaction. *Nanoscale* **2018**, *10*, 2231-5. DOI
44. Liu, Q.; Xu, Y.; Wang, A.; Feng, J. A single-step route for large-scale synthesis of core-shell palladium@platinum dendritic nanocrystals/reduced graphene oxide with enhanced electrocatalytic properties. *J. Power. Sources.* **2016**, *302*, 394-401. DOI
45. Ren, G.; Liu, Y.; Wang, W.; et al. Facile synthesis of highly active three-dimensional urchin-like Pd@PtNi nanostructures for improved methanol and ethanol electrochemical oxidation. *ACS. Appl. Nano. Mater.* **2018**, *1*, 3226-35. DOI
46. Lou, Y.; Li, C.; Gao, X.; et al. Porous Pt nanotubes with high methanol oxidation electrocatalytic activity based on original bamboo-shaped Te nanotubes. *ACS. Appl. Mater. Interfaces.* **2016**, *8*, 16147-53. DOI
47. Zhang, Y.; Wang, S.; Si, F.; et al. Synergistic effects of p-d orbital hybridization and $CeO_2$ surface engineering on PtBi nanoplates for methanol electro-oxidation. *Sci. China. Mater.* **2024**, *67*, 1975-84. DOI
48. Hu, X.; Xiong, H.; Dou, J.; Jiang, Z. Strengthening the activity and CO tolerance with bi-component PtNi/NbN-C catalyst for methanol alkaline electrooxidation. *Electrochim. Acta.* **2024**, *507*, 145092. DOI
49. Zhang, Z.; Luo, Z.; Chen, B.; et al. One-pot synthesis of highly anisotropic five-fold-twinned PtCu nanoframes used as a bifunctional

electrocatalyst for oxygen reduction and methanol oxidation. *Adv. Mater.* **2016**, *28*, 8712-7. DOI

50. Yuan, M.; Wang, C.; Wang, Y.; Wang, Y.; Wang, X.; Du, Y. General fabrication of RuM (M = Ni and Co) nanoclusters for boosting hydrogen evolution reaction electrocatalysis. *Nanoscale* **2021**, *13*, 13042-7. DOI
51. Hao, Y.; Wang, X.; Zheng, Y.; et al. Uniform Pt nanoparticles incorporated into reduced graphene oxides with $MoO_3$ as advanced anode catalysts for methanol electro-oxidation. *Electrochim. Acta.* **2016**, *198*, 127-34. DOI